Characteristics of Tsunamis Observed in Japan due to the Air Wave from the 2022 Tonga Eruption

Yuichiro Tanioka (tanioka@sci.hokudai.ac.jp)
Hokkaido University Faculty of Science Graduate School of Science: Hokkaido Daigaku Rigakubu Daigakuin Rigaku Kenkyuka Rigakuin https://orcid.org/0000-0003-3649-093X

Yusuke Yamanaka
Hokkaido University Faculty of Science Graduate School of Science: Hokkaido Daigaku Rigakubu Daigakuin Rigaku Kenkyuka Rigakuin

Tatsuya Nakagaki
Hokkaido University Faculty of Science Graduate School of Science: Hokkaido Daigaku Rigakubu Daigakuin Rigaku Kenkyuka Rigakuin

Research Article

Keywords: 2022 Tonga eruption, Air-sea coupled tsunami, Tsunami numerical simulation.

Posted Date: February 7th, 2022

DOI: https://doi.org/10.21203/rs.3.rs-1320093/v1

Abstract

A large eruption of the Hunga Tonga-Hunga Ha□apai volcano in Tonga on January 15, 2022 generated air-sea coupled tsunamis observed at the ocean-bottom pressure sensor network along the Japan Trench (S-net) in Japan. Initial tsunamis from the 2022 Tonga eruption, detected by 106 ocean bottom pressure sensors, were well modeled by an air-sea coupled tsunami simulation, with a simple atmospheric pressure pulse having a half-wavelength of 300 km and a peak amplitude of 2 hPa. A one-dimensional air-sea coupled tsunami simulation having a simple bathymetry shows that an input atmospheric pressure pulse with a short half-wavelength of 50 km, which is shorter than the length of the slopes, caused an amplitude increase via the Proudman resonance effect near the deep trench. The wavefront distortion due to the separation of the air-sea coupled wave (v=312 m/s) and sea wave (v= sqrt(gd)) is also significant near the shore. In contrast, these effects are not significant for the half-wavelength of the input atmospheric pressure pulse of 300 km. These results indicate that observing the wavelength of an atmospheric pressure pulse due to an eruption is important for forecasting the heights of air-sea coupled tsunamis.

1. Introduction

A large eruption of the Hunga Tonga-Hunga Ha□apai volcano in Tonga on January 15, 2022, caused devastating disasters in nearby areas. The eruption generated air waves coupled with seawater waves propagating through the Pacific. Tsunamis, long-waves in the ocean, generated by the air wave from the eruption were observed in tide gauges and ocean bottom pressure sensor network along the Japan trench (S-net) in Japan. The network, which includes 150 pressure sensors connected by a cable with 30 km intervals, is operated by the National Research Institute for Earth Science and Disaster Resilience (NEID) in Japan (Uehira et al. 2012; Kanazawa 2013). A maximum tsunami amplitude of 1.2 m was observed at Amami in Japan, and thus, a tsunami warning was issued by the Japan Meteorological Agency.

Similar air-sea waves had previously been generated by the Krakatoa volcano eruption in 1882 (Harkrider and Press 1967), and the authors indicated that the air wave propagated at a velocity of 312 m/s. This kind of air-sea coupled waves, which is often called to meteotsunamis, has already been studied without volcanic eruptions (Hibiya and Kajiura 1982; Fukuzawa and Hibiya 2020; Kubota et al. 2021). Saito et al. (2021) suggested that meteotsunamis are amplified when the velocity of the air waves is similar to that of the tsunami waves. This is called the Proudman resonance effect (Williams et al., 2021). In the case of the tsunami caused by the air wave from the volcanic eruption, the tsunami propagated near a deep trench should be amplified.

In this paper, the tsunami waves observed at ocean bottom sensors of S-net in Japan were modeled by the air waves generated by the 2022 Tonga eruption. We discuss the characteristics of tsunami propagation, including the tsunami amplification near the Japan Trench, which has a depth of approximately 8 km.

2. Data And Method

Ocean bottom pressure data observed at 113 sensors at S-net (National Research Institute for Earth Science and Disaster Resilience, 2019) were downloaded (Figure 1). The observed data are filtered in the periods between 100 and 3600 s using the bandpass filter in Seismic Analysis Cord (SAC) developed by Goldstein et al, (2003) (Supplement S1).

The governing equations to be solved by the numerical simulation is briefly explained. Linear approximation of Euler`s momentum equation is:

$$\frac{\partial u}{\partial t} = -\frac{1}{\rho}\frac{\partial p}{\partial x}$$

$$\frac{\partial v}{\partial t} = -\frac{1}{\rho}\frac{\partial Pp}{\partial y}$$

1

$$\frac{\partial w}{\partial t} = -g-\frac{1}{\rho}\frac{\partial p}{\partial z}$$

where *u*, *v*, and *w* are the velocity in x, y, z-direction, respectively, *p* is the pressure, *g* is gravity acceleration, and ρ is the water density. By using longwave, or shallow water, approximation, third equation in (1) becomes

$$\frac{\partial w}{\partial t} = -g-\frac{1}{\rho}\frac{\partial p}{\partial z} = 0$$

2

Then, pressure *p* is $p = -\rho gz + c$ where c is a function of x, y, and t. At the ocean surface where *z* is a wave height (*h*), pressure (*p*) becomes atmospheric pressure (p_0) which is an input for the air-sea coupled wave in this study. Pressure, *p*, then becomes $p = \rho g(h - z) + p_0$. The momentum equations (1) then become

$$\frac{\partial u}{\partial t} = -g\frac{\partial h}{\partial x}-\frac{1}{\rho}\frac{\partial p_0}{\partial x}$$

$$\frac{\partial v}{\partial t} = -g\frac{\partial h}{\partial y}-\frac{1}{\rho}\frac{\partial p_0}{\partial y}$$

3

Next, continuity equation of the linear long wave is

$$\frac{\partial h}{\partial t} = -\frac{\partial du}{\partial x} - \frac{\partial dv}{\partial y}$$

4

where *d* is the ocean depth. Momentum equations (3) for air-sea coupled waves and continuity equation (4) were numerically solved using a staggered grid system with an input of the atmospheric pressure gradient at each time step. The grid sizes of the numerical computation were set at 1.5 km in both x and y directions.

The atmospheric pressures observed at approximately 3000 points in Japan (Weathernews, https://jp.weathernews.com/news/38708/, 2022) showed that the pressure pulse (a peek amplitude of approximately 2hPa, and the duration of 20-15 mins) passed through Japan from southeast to northwest with a strike of -44°. The shape of the pressure pulse was assumed to be half the wavelength of sine wave. The half-wavelength was set to 300 km, which corresponded to a duration of 16 mins. The peek amplitude was set to 2hPa. First, numerical computation in one dimension with a constant ocean depth of 5500 m was carried out to obtain the steady state of air-sea coupled initial wave. The pressure pulse and the steady state initial wave are entered into the two-dimensional computational domain from the low boundary along the x-axis (Figure 2). The pressure pulse is continuously propagated in y-direction with a constant velocity of 312 m/s. The bathymetry was rotated 44° clockwise (Figure 1 and 2) to match a strike of the pressure wave from Tonga.

3. Results

Nine observed tsunami waveforms at stations, S6N12, S3N19, S3N20, S3N21, S3N22, S3N23, S3N24, S3N25, and S3N26 (Figure 2), are compared with computed tsunami waveforms (Figure 3). In supplement S1, the observed tsunami waveforms of 106 stations in the S-net are compared with computed waveforms. The absolute time of the computed waveforms was set to fit the observed and computed tsunami waveforms at S6N12. The computed ones well explain the observed maximum amplitudes and waveforms at all stations. For a typical tsunami caused by an earthquake, shoaling from the deep to the shallow ocean should cause an amplitude increase. A small shoaling effect can be seen for this air-sea coupled tsunami (Figure 3). The Proudman resonance effect (Williams et al., 2020; Saito et al., 2021) is difficult to identify from Figure 3. We performed a one-dimensional simulation on a simple bathymetry to clarify these effects.

4. One Dimensional Tsunami Simulation

A one-dimensional tsunami simulation was carried out to understand the tsunami waveform deformation due to the existence of a deep trench. A simple bathymetry was set to compute the tsunami (Figure 4): a shore 100 km away from the left boundary; a slope of 1/25 from the shore to 200 km away, where water depth is 8,000 m (trench); a slope of 1/12.5 from 200 to 400 km away, where the water depth is 5,500 m;

and a flat bottom from 400 to 900 km away. For an input of the atmospheric pressure pulse, three different half wavelengths, 50 km, 100 km, and 300 km, were tested for this simulation.

Figure 4 shows snapshots of tsunami waveforms every 200 s for each input wavelength. For a half wavelength of 50 km (Figure 4a), three snapshots from 600 to 1000 s clearly show that the amplitudes of tsunamis increased when the water depths increased to 8,000 m. This is due to the Proudman resonance effect suggested by Williams et al. (2020) and Saito et al. (2021). After 2,200 s, the shoaling effect from 8,000 m depth to the shore increased the amplitude of tsunami. Shortening of the wavelength by the shoaling is not obvious. However, the shape of the wave front is distorted. This is due to the separation of air-sea coupled wave (*v=312 m/s*) and sea wave ($v = \sqrt{gd}$).

For a half wavelength of 300 km (Figure 4c), three snapshots from 400 to 800 s show that the shapes of the waves are distorted with time, while the amplitudes of the waves are not significantly increased. In contrast, the shoaling effect from 8,000 m depth to the shore is clearly seen in both the amplitude increase and wavelength shortening. The distortion of the wavefront is visible but not significant.

The snapshots from a half-wavelength of 100 km (Figure 4b) show that the characteristics of the waveforms are between those for half-wavelengths of 50 and 300 km. Three snapshots from 600 to 1000 s show that the amplitudes of the tsunami increased slightly when the depth of the water increased to 8,000 m. The shoaling effect is also observed in both the amplitude increase and wavelength shortening. The distortion of the wavefront is also observed from 1400 to 1800 s (Figure 4b).

5. Conclusions

Initial tsunamis from the 2022 Tonga eruption observed at 106 ocean-bottom pressure sensors in S-net, Japan, were well modeled by the air-sea coupled tsunami simulation with an atmospheric pressure pulse having the half wavelength of 300 km and the peek amplitude of 2hPa.

A one-dimensional air-sea coupled tsunami simulation with a simple bathymetry shows that an input atmospheric pressure pulse with a short half wavelength of 50 km, which is shorter than the length of the slope (200 km), caused an amplitude increase by the Proudman resonance effect near the deep trench. The wavefront distortion due to the separation of air-sea coupled wave (*v=312 m/s*) and sea wave ($v = \sqrt{gd}$) was also significant near the shore. In contrast, when the half wavelength of the input atmospheric pressure pulse was 300 km, which is longer than the length of slops, the wave shape distortion due to those effects became small. It is important to observe the wavelength of an atmospheric pressure pulse due to an eruption to forecast the heights of air sea coupled tsunamis.

Declarations

Acknowledgements

We thank Dr. N. Y. Chikasada for providing us the information about his S-net data analysis. This study was partially supported by the Ministry of Education, Culture, Sports, Science and Technology (MEXT) of Japan, under its The Second Earthquake and Volcano Hazards Observation and Research Program (Earthquake and Volcano Hazard Reduction Research).

Availability of data and materials:

None

Competing interests:

None

Funding

This study was partially supported by the Ministry of Education, Culture, Sports, Science and Technology (MEXT) of Japan, under its The Second Earthquake and Volcano Hazards Observation and Research Program (Earthquake and Volcano Hazard Reduction Research)

Authors' contributions

Y.T. Overall research and computations

Y.Y. provided information about air-sea coupled wave analysis and discussed research objectives

T.N. processed observed waveform data

References

1. Fukuzawa, K., and T. Hibiya, 2020: The amplification mechanism of a meteo-tsunami originating off the western coast of Kyushu Island of Japan in the winter of 2010. J. Oceanogr., 76, 169–182. https://doi.org/10.1007/s10872-019-00536-3.
2. Goldstein P., Dodge D., Firpo M., & Minner L. (2003), SAC2000: Signal processing and analysis tools for seismologists and engineers, invited contribution to “The IASPEI International Handbook of Earthquake and Engineering Seismology”, Edited by W.H.K. Lee, H. Kanamori, P.C. Jennings, and C. Kisslinger, Academic Press, London
3. Harkrider D., & Press F. (1967) The Krakatoa air-sea waves: An example of pulse propagation in coupled systems*. Geophysical Journal International*, **13**, 149–159
4. Hibiya, T., and K. Kajiura, 1982: Origin of the Abiki phenomenon (a kind of Seiche) in Nagasaki Bay. J. Oceanogr. Soc. Japan, 38, 172–182. https://doi.org/10.1007/BF02110288.
5. Kanazawa T. (2013) Japan Trench earthquake and tsunami monitoring network of cable-linked 150 ocean bottom observatories and its impact to earth disaster science, Proceedings of the International Conference Underwater Technology

6. Kubota, T., T. Saito, N. Y. Chikasada, and O. Sandanbata, 2021: Meteotsunami observed by the deep-ocean seafloor pressure gauge network off northeastern Japan. Geophys. Res. Lett., 48(21), e2021GL094255. https://doi.org/10.1029/2021GL094255.
7. National Research Institute for Earth Science and Disaster Resilience (2019), NIED S-net, National Research Institute for Earth Science and Disaster Resilience, https://doi.org/10.17598/nied.0007
8. Saito T., Kubota T., Chikasada N.Y., Tanaka Y., & Sandanbata O. (2021) Meteorological tsunami generation due to sea-surface pressure change: Three-dimensional theory and synthetics of ocean-bottom pressure change. *Journal of Geophysical Research: Oceans*, **126**, e2020. https://doi.org/10.1029/2020JC017011
9. Satake K. (2015) Tsunamis, in treatise on geophysics, 2nd edn., vol 4, Elsevier, Amsterdam, pp 477–504
10. Uehira K., Kanazawa T., Noguchi S., Aoi S., Kunugi T., Matsumoto T., Okada Y., Sekiguchi S., Shiomi K., Shinohara M., & Yamada T. (2012) Ocean bottom seismic and tsunami network along the Japan Trench. In: Abstract OS41C-1736 presented at 2012 Fall Meeting, AGU
11. Williams D.A., Horsburgh K.J., Schultz D.M. et al. (2021) Proudman resonance with tides, bathymetry and variable atmospheric forcings. *Natural Hazards*, **106,** 1169–1194. https://doi.org/10.1007/s11069-020-03896-y

Figures

Figure 1

Location of ocean bottom pressure sensors in S-net (red circle) used in this study. The blue rectangle denotes the air-sea coupled tsunami computation area.

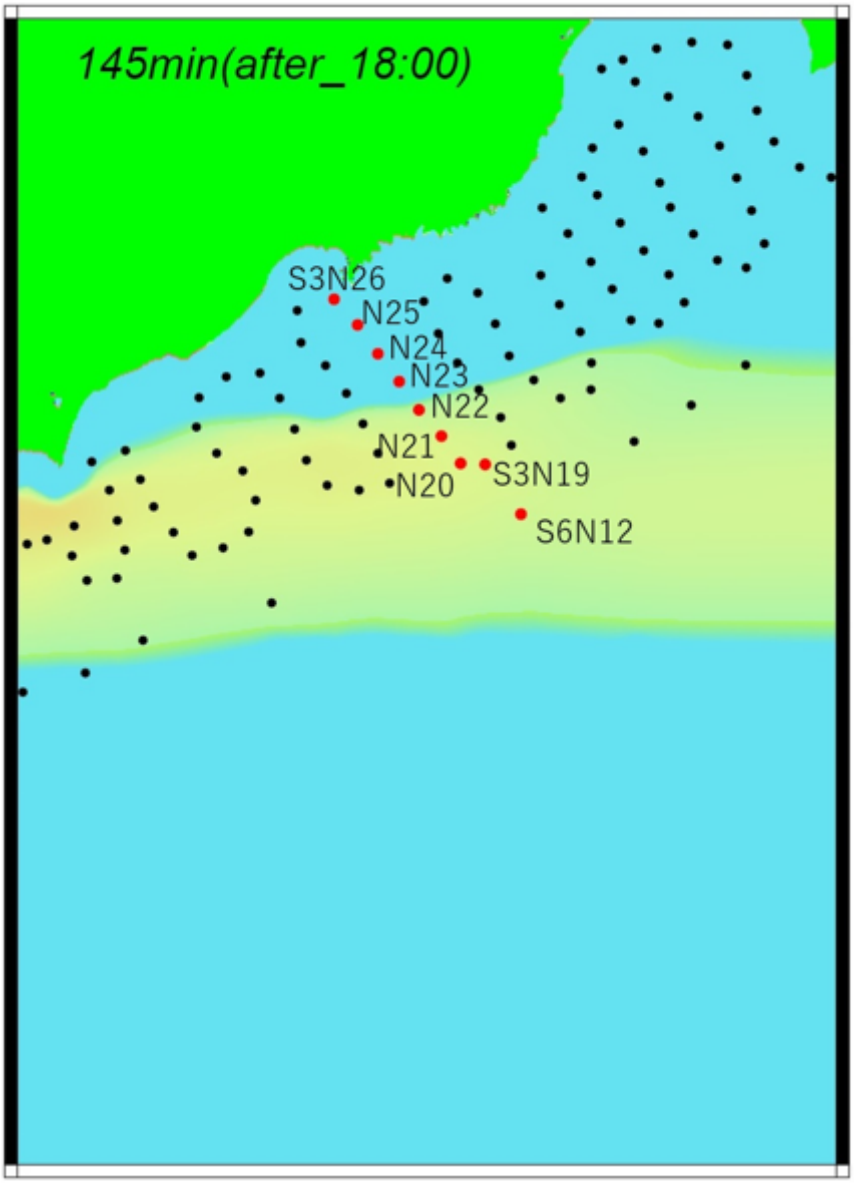

Figure 2

A snapshot of an air-sea coupled computed tsunami at 145 mins after 18:00. Circles represent the locations of ocean bottom pressure sensors used in this study. Red circles represent the sensors where observed and computed waveforms are compared in Figure 3.

Figure 3

Comparison of observed and computed waveforms at nine sensors is shown in Figure 2. Black lines represent observed waveforms, and red lines represent computed waveforms. Long period waves in the first 100 mins in the observed waveforms are an effect of the bandpass filter.

Figure 4

Ten snapshots of one-dimensional simulations for three atmospheric pressure pulses, half-wavelengths of 50 km (a), 100 km (b), and 300 km (c). The bottom shows a simple bathymetry used in this simulation.

Supplementary Files

This is a list of supplementary files associated with this preprint. Click to download.

- Supplementarymaterial.docx